An experimental and numerical contribution for understanding the in-situ shear behaviour of unreinforced masonry

Pratik N. Gajjar[1]; Elena Gabrielli [2]; Dafne Carolina Martin-Alarcon[1]; João M. Pereira[1]; Paulo B. Lourenço[1]; Camilla Colla[2]

[1] University of Minho, ISISE, Department of Civil Engineering, Guimarães, Portugal

[2] Alma Mater Studiorum-University of Bologna, DICAM, Department of Civil, Chemical, Environmental and Materials Engineering, Italy

Abstract: The assessment and modelling of unreinforced masonry structures require an adequate understanding of ma- sonry behaviour under shear loading. In particular, the behaviour of the interfaces connecting, brick and mortar, are of key importance during seismic actions. This is because the unit-joint interface may act as the main plane of weakness in the masonry composite. It has been observed that the inelastic behaviour of masonry structural elements subjected to shear loading depends largely on this interface behaviour. Hence, different experimental techniques available to observe in-situ or in a laboratory the behaviour of masonry under shear loading are reviewed and a suitable experimental campaign, also employing DIC as optical monitoring system is undertaken and shear tests are performed. After visualisation and discussion of novel displacement and shear strain maps and graphs, the experimental masonry behaviour is replicated via different numerical models based on the finite element approach. Models are used for better characterising the behaviour of the interface between brick and mortar. Further, the main parameters affecting the numerical models are discussed.

Keywords: Masonry, URM (Unreinforced Masonry), DIC, Experimental test, Shear test, Optical monitoring, Brick, Mortar, Interface, Numerical modelling.

1. Introduction

Due to the orthotropic nature of masonry, the bond between masonry units and mortar is usually the weakest link in masonry subjected to any action, as cracking and sliding concentrates mostly in the masonry joints. In the case of unreinforced masonry structures (URM) and seismic actions, masonry walls are usually subjected to in-plane and out-of-plane loading. For modern masonry walls, the tensile strength plays some role in case of out-of-plane effects. As an example, the European code for masonry structures [1] provides values for flexural strength having the plane of failure parallel to the bed joints (resulting typically from the tensile bond strength of the joints) and flexural strength of masonry having the plane of failure perpendicular to the bed joints (resulting typically from the shear bond strength of the joints with a toothed crack). Historical masonry structures subjected to out-of-plane loading exhibit usually brittle collapse as macro-blocks [2] and their capacity stems primarily from geometry and not from material strength. In-plane action of masonry subjected to combined vertical and lateral loading is the preferred mode to resist seismic actions, both in case of modern URM and historical masonry buildings, where ties or other measures are applied to avoid the brittle out-of-plane collapse. Therefore, the seismic assessment and modelling of unreinforced historical masonry structures require an adequate understanding of behaviour of masonry under shear loading.

Behaviour and evaluation of shear strength of URM under lateral loading are emphasised by the shear failure of a masonry wall. The failure can be achieved by lateral bed joint failure or diagonal shear cracking [3,4]. To define such behaviour and test masonry, many experiments were conducted either in-situ or at laboratory scale [5–7]. Depending on the objective of research, particular types of tests can be chosen. The in-situ test on masonry wall using flat-jacks can give important insight into the shear behaviour in its built environment [7], while the laboratory test offers more control over the experimental procedures. The former turns more complex in case of historical masonry structures as their walls are mostly built with multi-leaf cross-sections that impose additional sets of influencing factors on the experiment, such as the leaves' thickness and their amount of connection to each other [8–10].

Numerical models are generally assumed to adequately replicate the behaviour of the masonry composite, particularly the behaviour of masonry joints under shear loading. Various modelling techniques are available to model masonry's discontinuity, such as detailed micro-models and meso-models [11,12]. Depending on the level of complexity of the constitutive models, the micro-models can

show detailed stress analysis as well as various failure mechanisms. However, these models are only so accurate as the information introduced as input from experiments, documentation, and codes. Considering the unique complex nature and variety of existing masonries, structures and multiple affecting factors, such as boundary conditions, amplitude and frequency of lateral load, the different material properties influence the walls' and global behaviour of a structure [13]. Thus, predicting and defining their mechanical behaviour becomes difficult even considering only in-plane actions. Hence, simplified numerical approaches are often used. For example, masonry is assumed as a homogeneous material, which in turn requires classification of behaviour of masonry units and interfaces [14,15].

Simplified modelling approaches such as micro-models are particularly suited to observe the behaviour between brick units and mortar. Micro-models differentiate the units, mortar and interface in the models; furthermore, they allow to establish a relation between average masonry stresses and strain. As the mechanism appearing between masonry units and mortar is highly complex and influenced by various factors, most investigations that analyse this mechanism are phenomenological and applied to individual case scenarios [16]. Overcoming these strong limitations present in this scientific research field and in assessment activity in the engineering praxis, would be highly desirable, having also in mind how urgent and vast would be the need to take better and proper care of URM structures and heritage. Much more, in the light of now-established worsening trends of climatic change, the constructions are more often undergone to extreme events and exceptional loading, thus making the need for mechanical behaviour assessment and the understanding of real state of health even more important and frequent.

Therefore, the goal of this work is to improve the understanding of masonry behaviour under shear loading. In particular, the paper addresses the shear behaviour of the bedding mortar joint-brick interface and the techniques available for testing and numerical modelling. For these purposes, experimental shear testing, optical monitoring via digital image correlation and nonlinear numerical analyses are employed. Novel maps obtained from the shear test via optical micro-monitoring are aimed at visualising the displacement and strain fields and so to gain an improved understanding of local behaviour of masonry subjected to in-plane loading.

For numerical analysis, two types of micro-models are considered, namely detailed micro-models and meso-models. The purpose of these models is to replicate the observed mechanisms and behaviour of the test unit, in agreement with the experimental results and to better understand the fracture process

involved in masonry shear joint failure. This will assist in defining the key interface parameters playing a role, when masonry is subjected to in-plane loading.

2. Shear tests for the masonry joints

The test types described in the following can be applied to small masonry sections or specimens consisting of few units, in order to understand the shear bond strength of masonry units. By means of these tests, it is possible to characterise different parameters that aid in masonry modelling and assessment, such as cohesion, friction angle and dilatancy angle. However, due to the nature of these tests, uniform distribution of both the normal and shear stresses cannot be achieved [17]. Therefore, some degree of inaccuracy must be taken into account, given that a pure shear stress distribution in a masonry joint cannot be applied [18].

2.1 ASTM C1531 (In-situ shear testing)

The qualitative shear strength of mortar joints can be obtained following the procedures established in the ASTM C1531. According to this standard, the average in-situ mortar joint shear strength is obtained from experiments and calculations. Once preceding inspections and diagnostic investigations have been conducted on the construction and once a proper testing area is selected in an existing masonry wall, the test can be undertaken focusing on an unreinforced solid unit or an ungrouted hollow masonry unit. To comply with the standard procedure, the mortar joints of the testing area must be parallel to one another. Furthermore, it is advised to perform this test away from the mechanical influence area of openings or wall ends [19].

The ASTM C1531 standard allows three different methods; of these, method A will be further analysed here. The three methods differ mainly in how the normal compressive stress is controlled and how the vertical load is applied to the test unit. Method A controls the normal compressive stress and uses double flat jacks inserted two masonry courses above and below the unit to be tested. This ensures a predetermined value of the normal compressive stress on the masonry joints. Each of the two masonry units to the left and right of the tested unit are removed in order to place a horizontal hydraulic jack on one side and to leave a void on the other side. The hydraulic jack exerts the in-plane shear force providing the loading on one head of the test unit. To apply a uniformly distributed load, a stiff bearing plate with neoprene padding for better contact is added between the jack and the unit's head area, in

order to avoid punching failure of the unit. The horizontal displacement caused by the jack is monitored throughout the experiment via the use of linear variable differential transformers (LVDTs), mechanical extensometers, strain gauges or other electronic devices to accurately measure displacement, that is the unit's horizontal sliding (ASTM C1531-16, 2016). The intended amount of sliding causing the failure at the interfaces is usually a fraction of a millimetre. Generally, two LVDTs are used to instrument the test area, one placed between the test unit and the unit beyond the empty space created by removing a brick (front LVDT); the second is placed between the test unit and the unit behind the jack (rear LVDT), as shown in Fig. 1. The front LVDT monitors the intended forward sliding of the test unit along the mortar beddings due to horizontal loading. The rear LVDT is used as a control measure of possible backwards movement of the brick behind the hydraulic jack. In existing real walls and historical masonry, this event cannot be excluded due to imperfect workmanship by masons [20]. Whichever of the two bricks slides first, the test is considered concluded.

Regarding the alternative testing possibilities proposed by the testing standard, method B does not use flat jacks for controlling the normal compressive stress. Instead, it estimates the average compressive stress at the test unit by considering its relative location and the expected vertical load applied (Fig. 2a). Method C is the simplest method of the ASTM C1531 as it only requires the removal of the vertical head joints on both sides of the test unit (Fig. 2b). In one side, a small flat jack is vertically placed and sized to prevent applying load to the mortar joints instead of the test unit only. Similar to Method B, the normal compressive stress at the location is only estimated. In both methods, the horizontal displacements can be measured as for method A.

2.2 Couplet test

The couplet test specimen consists of two bricks joined by a single mortar joint. The specimen must be properly fixed to ensure that the resulting shear force acts along the plane of the joint. A two-point vertical compressive load, $F_{N1\text{-}2}$, acts on a steel beam in order to evenly distribute the load and balance the moment induced by the shear load [21]. This vertical load is applied gradually to a specified load, after which the vertical load is, ideally, kept constant for the rest of the test. Subsequently, keeping constant the vertical load, a horizontal shear load, F_S, is evenly distributed and applied on the bottom brick (Fig. 3a).

2.3 Triplet test

The triplet test uses three bricks joined by two mortar layers. The shear loading, F_S, at the bottom of the test scheme, is applied as a point load at each quarter of the unit brick height to ensure the resulting shear force develops along the two surrounding bed joints and rotation is reduced. This is aided by properly fixing the movement of the top and bottom bricks by using steel plates as rigid supports (Fig. 3b). This test setup still introduces important bending effects after the onset of failure of the first (and weaker) joint, which must be minimized by adequately fixing the specimen. The second (and stronger) joint fails at a later stage and the results must be carefully analysed in the post-peak phase, should this information be used [17]. Normal compressive strength, F_N, can also be added to the test in a manner similar to ASTM C1531 Method A. This is the standard laboratory test on new materials used in many countries, given its simplicity (e.g. Ref. [22]. Similar to other tests presented in this section, the shear resistance may be obtained for different pre-compression normal load levels, allowing to calculate the cohesion and friction angle.

2.4 Van der Pluijm test

The Van der Pluijm test [18] has an advantage over the couplet and triplet tests. This type of test allows a constant normal load, F_N, to be maintained upon shearing but without flexural effects. The Van der Pluijm test places two masonry units with a mortar joint unto two L-shaped solid steel moulds (Fig. 3c). This test introduces the shear force, F_S, directly on the joint, thus, making the bending moment in the joint equal to zero. Obviously, due to equilibrium conditions, the shear stress at the joint edges must be zero, meaning that a uniform distribution of shear stresses will not be found. Still, the point of application of the shear load, FS, and the overall arrangement of the test prevent flexural effects and the usual combination of non-uniform normal stresses and non-uniform shear stresses.

3. Experimental mortar joint shear testing

Sampling small and representative portions of masonry on-site for laboratory testing is rather complex, almost impossible, particularly when dealing with historical masonries, which may present weaknesses of materials, interfaces and other points. Unintentional damage of the sample may easily occur during sampling, handling or transportation operations; then, in the laboratory, sample preparation before testing would also have to take place. Moreover, as described in the previous

paragraph, geometry of couplets and triplets must be very specific and precise in order to avoid or limit unwanted factors influencing the test outcome figures. Thus, for multiple reasons, when interested in me- chanical properties and behaviour of existing or historical structures, it would always be advisable to employ testing techniques applicable on site, with minimum disruption of local loading conditions of the ma- sonry element to be tested. For this reason, the experimental section of this research work has considered a type of testing not requiring sampling and easily applicable in-situ.

This section describes the specimen, methodology, test phases and results obtained in the experimental evaluation of the mortar joints' shear behaviour in a masonry wall specimen, using ASTM C1531 as the basic guide. The experiment was performed in spring 2016 at the Laboratory of Structural and Geotechnical Engineering (LISG) of Bologna University, in Bologna, Italy. One brick masonry wall was used to perform shear tests at the mortar joints, at the same time employing innovative optical monitoring procedures. Besides the usual force-displacement data acquisition instrumentation, during the various test phases a 3D digital image correlation (DIC) system was also employed in order to properly capture the fine displacement and strain fields at the brick-mortar joint interface. Such outcomes were firstly necessary for improved mechanical understanding of masonry shear behaviour mechanism but also for the later part of this work, the numerical modelling.

3.1 Description of the test specimen and equipment

The masonry specimen used to perform the shear tests is a two header-thick wall with transversal brick connections. Made of new solid fired-clay bricks and natural hydraulic lime mortar joints, built almost 6 years prior to the experiments presented herein, the full-scale masonry laboratory wall follows typical Italian construction practice. It is fabricated to a height of 20 brick masonry courses with nominal 1 cm thick mortar joints. The masonry layout alternates full courses of stretcher bricks with courses of stretchers and headers connecting the two leaves of the wall.

During summer periods only, the masonry wall had been exposed to moisture capillary rise by tap water at the footing, in outdoor weather in Bologna, for 6 summers (approximately from end of May to beginning of October). The capillary rise and natural climatic exposure were aimed to cause ageing of the wall materials by cycles of evaporation and salt crystallisation as it would happen in a real, existing or historical wall construction. Due to the lack of outdoor exposure during winter periods, the specimen was not subjected to other weather damage, such as freeze-thaw cycles.

The nominal dimensions of the bricks and mortar joints are reported in Table 1 along with the measured dimensions of the test unit used in this experimental section. The properties of the masonry brick units and mortar were obtained by testing the constituents' materials individually. Several masonry units were tested along with mortar prisms in order to identify the material properties in as-built conditions. The average results can be seen in Table 2 [23].

Furthermore, the results of an axial vertical compression test per- formed on one representative wall specimen (dimensions of 500 × 450 × 120 mm^3) can be seen in Table 3. This wall was built at the same time and with the same materials as the wall tested in the experiments described herein [24].

Following the ASTM standard C1531, the test unit was first isolated at the left and right sides from the adjacent bricks in its brick course. Not to cause unwanted damage in the test area, the removal of adjacent mortar layers and bricks was first achieved by careful driller perforations gradually demolishing the mortar joints around the edges of the bricks to be removed (see Fig. 4), in order to separate as much as possible these bricks from surrounding masonry, lastly finishing off by chisel and hammer leverage action. Any remaining bits of unwanted mortar along the voids would also be gently removed by chisel. The test unit remained connected via mortar joints to the back leaf of the wall and also to the upper and lower courses in the front leaf of the wall.

The shear test experimental setup can be observed in Fig. 5. Two shear tests have taken place in sequence, in the same wall. First, a brick test unit was selected at the 16th course counting from the wall's bottom (Fig. 5a). Subsequently, a second test took place at course 6.

The wall was set up to sustain a distributed constant vertical loading along its full length in order to replicate the boundary conditions that would be typically found in a large masonry structure. Accordingly, a steel beam was placed on the top of the specimen wall (Fig. 5b) to distribute the vertical force of two vertical hydraulic jacks. Different values for vertical load were envisaged to allow defining the cohesion and friction angle of the masonry.

The test unit (a stretcher brick) was subjected to horizontal loading using a hydraulic jack connected to manual pump with pressure gauge. The two openings left by removing the lateral bricks allowed having the required space for the later sliding movement of the test unit and for placing the hydraulic jack, respectively. The hydraulic jack was levelled to the test unit using steel and rubber plates of similar dimensions to the brick's header, avoiding to load the mortar bed joints. These bearing plates were

placed in between the jack and the test unit and allowed distributing the load of the jack on the test unit's head. Another steel plate was added to the rear of the jack to distribute the load on the brick at its opposite end (reaction unit). At the rear, the steel plate extended into the upper and lower brick courses above the cleared hollow space (Fig. 5b): the greater distribution of applied force at the rear brick was intended to provoke the sliding of the front brick, where force was more concentrated and where the area was monitored via DIC. Finally, lateral confinement was applied to the wall by the use of structural steel plates and profiles with tension bars.

Non-destructive techniques are often preferred to test or monitor the historical masonry given their advantages in preserving the materials and cultural heritage in particular, and because not requiring restoring nor re-establishing the original material after use [13,25]. Among the different available non-destructive monitoring techniques, DIC (Digital Image Correlation) was selected because it is contactless, of rapid and relatively inexpensive application, as well as for its advanced diagnostic imaging capabilities. In this specific case, a 3D DIC system was used for capturing full-field data on a portion of the wall's front surface. Whilst DIC cases of use are numerous today for monitoring for example composites behaviour on masonry support [26], DIC's applications to plain loaded masonry alone are still few and considered innovative. DIC has hown to be effective in monitoring the global and local behaviour of masonry during mechanical experiments [27–29] as well as in assessing the mechanical behaviour of other anisotropic construction materials under load, such as timber [30].

The 3D DIC monitoring system used in the experiments described herein, consisted of a tripod set with two photocameras connected to a laptop with dedicated acquisition card and software. The cameras placed not perpendicular to the wall surface allow to obtain a stereo vision configuration producing 3D information about the observed material surface (Fig. 6a and b). The first couple of photos is recorded at zero loading and will serve as a reference. Subsequent couples of photos, shot with user-defined frequency during monitoring, will be compared with the initial images by specific software employing point-tracking algorithms. In fact, according to the technique's prescriptions, the monitored area (in these shear tests, the area around the tested brick) is prepared by coating the surface in white and overlaying a random pattern of black dots. These dots will be exploited by the data post-processing software in order to reconstruct the fine geometry of the monitored surface as well as for visualising displacement and strain maps. An innovative DIC procedure that overcomes the need for surface

preparation also exists, as previously developed by Colla and Gabrielli with the aim to exploit the non-destructive and non-invasive character of this optical method, particularly suitable for the cultural heritage and historical structures fields [31,32]. However, in the shown experiment the conventional coating procedure is adopted. The schematics of the DIC test setup can be seen in Fig. 6a and b, while the full test setup can be seen in Fig. 6c.

During the experiment, the loads applied through the vertical and horizontal hydraulic jacks were recorded using load cells and pressure gauges. The displacement monitoring was also carried out via hardware equipment by means of the 2 LVDTs prescribed by the testing standard. These were connected to the test unit and to the brick at the back of the jack. The latter was used as a control tool to measure any undesired displacement of the rear brick which would indicate a sort of flaw in this particular testing, given that in order to obtain maximum possible resolution via DIC, the monitored field focused around the front brick. The LVDT located on the test unit (front LVDT) was used to double-check on the sliding movement of the test unit along its mortar joints, allowing comparison with the outcome from the DIC system and for calibration of the numerical models.

3.2 Test results

From a preliminary test to check the efficacy of the setup, performed close to the top of the masonry wall (16th layer) with a horizontal compressive load reaching over 270 kN, an explosive failure mode was observed (Fig. 7). This, although the shear load was very gradually applied. The visible cracking and out of plane movement of some of the bricks show the extent of damage observed in this test (Fig. 8). In addition to the complete removal of the test unit, the applied lateral load has also caused sliding of adjacent brick units. A considerable amount of sliding was also observed near the reaction point at the rear of the horizontal jack where initial measured displacement was about double than the one measured at the test unit (Fig. 7).

This unexpectedly abrupt, brittle behaviour could be explained by the increase in the lime mortar strength due to prolonged water intake (by moisture capillary rise and especially by rain precipitation) in the wall during the summer ageing periods. It is well known that lime mortar has a much slower setting and longer strength development time than cement mortars. Thus, even if moistening of the mortar during outdoor exposure has started a number of months after wall construction, the mechanical beneficial effect was not negligible. This has not only brought to a high resistance mortar but also to

hardening, characteristics observed in new, modern, cement mortar. It has been previously reported an increase in strength and stiffness of lime mortar samples undergone to similar ageing cycles as the above-mentioned ageing [23]. Thus, usefulness of this preliminary test lays also in observation of possible different test responses in the case of historical, decayed or deformable mortar joints (curve showing softening before failure, as it will be seen in the following shear test at course 6) compared with stiff, high-strength mortar joints (showing brittle behaviour and little deformation up to peak load) as seen in this test at course 16 and as it could be encountered in new masonry constructions. Indeed, this could add difficulty in performing this type of test.

To overcome this type of failure, before performing the next shear test at the 6th layer of the wall, several modifications were introduced (Fig. 9). On one side, the vertical load was entirely removed to ease the sliding of the test unit; on the other side, to reduce the area of the failure planes and thus the necessary applied horizontal force, only half of a brick was considered as test unit. This was obtained by separating the stretcher brick into 2 parts by a groove, approximately 11 mm wide. The groove also extends into the mortar bed-joints (Fig. 9a). This procedure separated the test unit into two distinct pieces of approximately half brick size.

The exact time sequence has foreseen, at first, the removal of the 2 bricks at the left and right side of the test unit, similar to what was seen for the test at course 16 (Fig. 9b). The mechanical operation was again undertaken by stitch drilling and chisel, as seen previously (Fig. 4). Then, in the wall's second or rear leaf, the brick adjacent to the test unit was also carefully removed, leaving the test unit connected only to the upper and lower course's bricks via its top and bottom bed joints (Fig. 9b). Further, the test unit was carefully halved by stitch drilling and masonry surface was prepared for optical monitoring by white paint coating and black speckles pattern (Fig. 9c). Finally, to prevent sliding or cracking in the brick behind the jack, the hydraulic jack was rested with its back against a stiff steel plate (Fig. 9d) and connected to hydraulic pump; the LVDT was mounted as last (Fig. 10).

The obtained test unit resisted a maximum horizontal loading of 57 kN before its failure. It failed along the interfaces and slid along the bed joints. At the end of data acquisition, a final displacement of 7.4 mm was recorded for the test unit (Fig. 11a). The series of yellow arrows indicate the direction of the load and the area on which the load was applied on the brick head. Unlike the previous shear test at course 16, this test at course 6 did not show a sudden brittle behaviour, as it can be observed in the

first part of the in-plane load-displacement diagram presented in Fig. 12. This difference could easily be explained by both the introduced modifications in setup and by the lower position of course 6 in the wall. Compared to course 16 (only affected by rainwater absorption and its evaporation, with limited salt crystallisation causing mortar decay), course 6 underwent many more additional cycles of water evaporation and crystallisation, while moisture capillary rise did not reach course 16. In Fig. 12, the curve is obtained from LVDT data. It can be seen that at the peak load of 57 kN (the end of test according to masonry shear strength determination by sliding, as described in ASTM C1531), the measured displacement is between 0.2 mm and 0.3 mm. Such considerably larger displacement measured at this course 6 for a much smaller maximum load (57 kN) compared to values recorded for the case of testing at course 16 can be equally related to motivations provided just above in text.

Fig. 11b shows a schematic of Fig. 11a, highlighting the involved mortar joints, test unit and active sliding interfaces. Their identification was not done as much from Fig. 11a, as from observation of later-presented displacement map in Fig. 14. The same 2 sliding surfaces were entirely involved at the initiation of sliding, coinciding with maximum load.

The experimental data obtained from the DIC monitoring of the test area were the spatial coordinates of each pixel in the images, at each time instant throughout the test. From these, surface geometry, displacement as well as strain values can be determined for each pixel of the whole monitored area. Thus, the distribution of each parameter can be plotted as full-field maps. Of great interest is the distribution of shear strain in the observed x-y plane at maximum load during the experimental test. It clearly shows that the shear strains are well developed along the length of interfaces of brick and mortar joints (Fig. 13). According to the colour linear legend visible at the top of the image, the maximum concentration of shear strains is primarily observed close to the mortar layers. This can be expected due to the inferior mechanical properties of the mortar compared to the brick material. At first sight, it would appear that the greater deformability of the mortar allows for accommodating the majority of shear strain in the joints. In the bottom joint, at this later phase of loading, the good quality of the interface allows a portion of the bottom brick (from 5th wall layer) to engage in the resistance mechanism. At the top joint, the top brick (from 7th wall layer) on the contrary appears to play only a very limited resistance involvement. Also, note that at this joint, the mean value of shear strain is 57% greater than at the bottom joint.

The displacement distribution values at maximum loading before failure can be observed in Fig. 14. The obtained map is interesting as it shows how the test unit is considerably displaced (purple colour in the linear colour legend indicates maximum displacement values, that is between 0.27 and 0.29 mm) while the top mortar joint has remained almost idle (orange-red coloured area) with only the lower interface of this joint showing displacement towards the brick sliding direction. A different behaviour is noticed in the bottom mortar joint, where a major part of the joint is observed to move along with the test brick (purple and violet coloured area of the bottom joint). It involves at least a little, in the displacement a considerable part of the brick beyond the joint, at the 5th layer (amber and orange coloured, that is between 0.018 mm and 0.053 mm of displacement, so a very limited displacement). In the case of this joint, the shape of displaced area seems intending to form a failure plane across the mortar joint thickness, something that did not seem to have happened, see Fig. 11a. In fact, the right edge of this mortar joint still shows much smaller displacement (amber and green joint coloured areas) than the rest of the joint.

Thanks to the use of 3D optical monitoring, for the first time the production and observation of full-field parameter maps have allowed a detailed insight view into the shear mechanisms in masonry at micro-scale. The vision of sub-millimetric distribution of mechanical information over the area of interest enables to view and read what happens at the shear sliding interfaces.

After the above discussion of parameter maps, it is still worth adding and underlining some considerations. From in-plane displacement map it becomes clear that displacement values vary strongly across active interfaces and not all 4 interfaces are active. Rather, it appears that, up to maximum shear loading, only the length of one full interface is active per each mortar joint in contact with the test unit. As visible in Fig. 15 - where Figs. 14 and 13 are directly compared and overlapped with the geometry configuration (white dotted lines) obtained at the end of data recording (Fig. 11a) - in the top mortar joint the lower interface is active for its full length; in the lower joint the lower interface is active for about three quarters and for about one quarter the higher interface is. This may be due to construction factors such as workmanship or material factors. Further, a short distance away from the active sliding interfaces, the test unit and joints show an undisturbed, homogeneous displacement field. Not even the change of material is recognisable from the colours (Fig. 15a).

By newly inspecting the shear strain map, it can be inferred that the higher strain concentration noticed at the top side of the test unit could be explained by slightly eccentric loading on the unit's head (Fig. 15b).

This would not be due to unprecise positioning of the jack. Instead, as seen earlier by noticing which interfaces are active, the sliding block is not formed by the test unit only, as the bottom mortar joint remains adherent to the unit. If the centre of mass of the sliding brick was expected to be at the centre of the brick area, due to the bottom joint the centre moves lower. However, the horizontal distributed load remains applied on the intended brick lateral face, thus with a resulting force having an application line passing higher than the centre of mass of the sliding block. Vicinity of the shear load to the top active interface and the involvement of a consequent possible rotation mechanism of the unit may well explain the higher value of shear strain at that position.

After having studied the shear phenomenon near peak loading, in order to study also the shear behaviour after peak load, the ongoing of DIC displacement curves from some points selected along the full length of an interface are plotted and compared throughout the full recording time of the test against the values from the LVDT (Fig. 16). The five locations of data extraction (Fig. 16a) are DIC points along the interface between test unit and bottom layer of the mortar. The graph shows that the DIC values are independent from the measurement position along the joint as a result of a rigid body sliding (Fig. 16b). Further, the DIC displacements coincide with the LVDT values in terms of time of occurrence of sliding while, after the first sliding step (occurring just after 400 s on the X-axis), the absolute displacement values measured by DIC and LVDT differ. In the final sliding phases, the graph shows about 15% greater sliding for LVDT, that is a greater sliding for the brick than for the upper part of the lower joint. This is also testified by the white contour of final configuration reported in Fig. 15, where the test unit, although fully joined to the bottom mortar joint (length of contact surface looks the same for brick and joint) appear to have slid further forward. Crushing is noticeable at the active interface of this joint, only (lower surface), by the wobbling white contour. The reason for this difference in the graph is that the LVDT displacement is measured at mid-height of the brick. However, as described earlier, the active interfaces at the top and bottom of the test unit define an asymmetrical sliding-block shape, where the fixed point of the LVDT is no more in barycentric position.

Further, the higher strain observed at the top active interface may have caused the top interface to start breaking first, causing a small anticlockwise rotation of the brick block, together with forward sliding translation. Such rotation of the test unit and the crushing of the top and bottom joints is clearly noticeable at end of sliding in their lower portions (white contours in Fig. 15). In this case, the LVDT is likely to have measured higher displacement values than the points in lower position, as visible for the LVDT curve in the graph of Fig. 16b. Therefore, the DIC results at the interface are a better representation of the response exhibited by the test unit. To be also considered that while it would not be possible or not recommendable to fix a real LVDT over the interface because it may detach before the end of testing, it is always possible in recorded optical data to select endless DIC points over an interface and use them as virtual LVDT points. This is another relevant advantageous aspect of optical monitoring application.

It should not go unnoticed that before occurrence of the first sliding (at approx. 400 sec in Fig. 16b), curves from the 2 types of recording systems – DIC, LVDT - overlap perfectly also in terms of absolute values. This is proof of reliability for DIC measurements. A final important consideration that can be drawn from observing the curves ongoing in Fig. 16b is the step-like distribution of values, alternating steep vertical segments with horizontal ones. This ongoing seems to point to a discontinuous sliding, progressing by sudden laceration of portions of the interfaces alternated to rest periods with possible accumulation of additional fracture energy.

4. Numerical modelling: Micro-model

Using DIANA 10.3 finite element software [33], a series of numerical models of the test unit were created to simulate the structural behaviour observed during the described experiment at course 6. The purpose of these models was to replicate the observed mechanisms and behaviour of the test unit in agreement with the performed experiment, in order to better characterise the phenomena and the involved relevant parameters while using in-situ shear testing. The visualisation of the inelastic behaviour of the joint in the test unit was of key importance for the models and was modelled by means of a nonlinear constitutive interface model. The experimental shear test was modelled with different approaches: the micro-model and the meso-model. This section only addresses the micro-model, whereas the meso-model is later addressed in section 5.

The constitutive model adopted for the analysis is based on the theory of plasticity. As such, following the multi-surface plasticity theory, a composite yield surface defines the different possible masonry failure modes [34].

4.1 Model description

The micro-model consisted of the test unit where the horizontal load is applied, plus two full bricks on the bottom and top, and two mortar joints (Fig. 17a). The boundary conditions used in these micro-models are presented in Fig. 17b. Because there was no vertical pre-compression and the self-weight was marginal when compared with the remaining acting forces, the upper and lower full bricks were constrained in their free edges. Also, the modified size of the single-leaf test unit (125 mm in length) compared with adjacent full-size brick units attached to the second leaf justifies the selection of the assumed boundary conditions. In the numerical model, the applied in-plane load was simulated as a force distributed along the right vertical face of the test unit similar to the real test situation.

In this model, bricks and mortar were kept as linear-elastic materials with properties as from Tables 2 and 3. They were represented using continuum elements. The planes of failure observed during the experi- ment were represented by means of discontinuous interface elements and nonlinear inelastic properties. Given that the experiment was performed on a masonry panel, plane stress elements were used to simulate the test.

The brick and mortar were both meshed with the Q8MEM plane-stress element. This is a four-node quadrilateral isoparametric element based on linear interpolation and Gauss integration [33]. The mortar joints of masonry are a geometric discontinuity and their interface is the most probable fracture plane. As such, the behaviour of the interface was of particular importance. In the experiment, the masonry test unit failed at the interfaces joining mortar with test unit (top interface) and mortar with bottom brick unit (bottom interface), as in Fig. 18.

The interface elements were specified as L8IF elements and introduced into the nodes of the model after the meshing of the brick and mortar was completed. The L8IF element is based on linear interpolation and a 2-point Newton-Cotes integration scheme is then applied by DIANA [33]. To calibrate the numerical model for the initial stiffness of the interface, linear static analyses were carried out. The elastic parameters of the interface were calibrated to reproduce the experimental stiffness of the joint. From the range of normal and shear stiffness values, 100 N/mm^3 and 45 N/mm^3 were chosen

respectively, as those values were better able to reproduce the initial stiffness of the experimental test. These values are in the range generally found for masonry [35], with a normal stiffness in the range of 10-100 N/mm^3 and a shear stiffness about 40% of the normal stiffness.

The nonlinear behaviour of the interface elements was modelled using a multi-surface plasticity model. The so-called Combined Cracking-Shearing-Crushing (C-S-C) constitutive model can simulate all the basic failure modes of masonry such as fracture, frictional slip and crushing along the interface [33]. In fact, the C-S-C model expands from the Coulomb friction model by adding a tension cut-off and an elliptical compression gap, as shown in Fig. 19. All of the modes present in C-S-C would experience softening; however, only the elliptical compression cap mode experiences softening preceded by hardening. The most relevant aspect of this criterion for the problem at hand is the advanced implementation of the shear behaviour. The model was again updated by fitting to the experimental results and the material properties can be observed in Table 4. The recommendations from Ref. [36] were used for the unavailable inelastic properties. The compressive part of the model was not used, as compressive stresses remain at very low level.

4.2 Micro-models results

The comparison between the experimental load-displacement diagram and the numerical C-S-C model can be seen in Fig. 20. The location used to extract the displacement is the same where LVDT was attached during the experiment. In-plane load represents the force obtained with load cell connected to the hydraulic jack used to apply the horizontal oad during the experiment and in-plane displacement refers to the displacement observed experimentally via LVDT. From the figure, it can be observed that the C-S-C model allows an adequate representation of the experimental response in the elastic and inelastic ranges.

Fig. 21 presents the in-plane displacement (Fig. 21a), shear stress (Fig. 21b) and shear strain (Fig. 21c) observed at the peak shear force. From Fig. 21a, it can be noticed that the in-plane displacement is primarily concentrated at the right-side of the half-brick given the sliding at the upper and lower interfaces. Fig. 21b & c shows that the shear stress and strain are focused near the top and bottom mortar layers, which are identical in terms of distribution values but mirrored in sign due to the shear action.

Fig. 22 presents for two distinct time instants the shear stress distribution along the upper interface for the interface model considered for the analysis. Here, only the distribution at the upper interface is presented because the distribution observed at the bottom interface is similar. The reduction in magnitude at ultimate condition is due to the loss of the bond, expressed by the cohesion. It is also noticed that the shear stress distribution is not symmetric, with higher values at the side of the load application. This is due to the rotation of the unit shown in Fig. 21a. Finally, peaks are observed in the edges of the unit, which are due to the boundary effects and local increase of normal stress.

5. Numerical modelling: Meso-model

A meso-model discretises the continuum into particle structures for different materials, aiming at better understanding the fracture processes of quasi-brittle materials. The particles may be linear elastic and assembled with respect to a Voronoi tessellation by creating a lattice model connection by inelastic interfaces. This tessellation divides a plane within its given boundaries into various polygonal regions (particles) with a centre (nuclei) [37]. Thus, the particles are interconnected to one another on their surface planes, by nonlinear interfaces. As such, all of the inelastic phenomena of the model occur in the interfaces surrounding the particles. The fractures that occur in the interface consist of progressive bond breakage of the interface [37].

The particles are assigned an average size and a distortion factor to control the shape irregularities [38]. The nuclei of the particles are chosen and, within the convex polygon, each of the points is closer to the nuclei of the polygon than to any other surrounding nuclei. The geometry and material properties are created and assigned to each section of the model. Then, a continuous element mesh is created within all the particles and a separate interface element mesh around each particle.

The frictional constitutive model used for the meso-model was the C- S-C constitutive model used to model the interface elements described in section 4. The meso-model was constructed utilising the various C-S-C nonlinear parameters defined in Table 4.

5.1 Model description

The meso-model was created using similar boundary conditions and loading as in the micro-modelling of Section 4. In order to model the experimental shear test adequately, its individual components were first calibrated as in Ref. [38]. As the meso-model is phenomenological, the mortar

and brick were modelled individually as 100 × 100 mm^2 samples. These samples were then subjected to elementary tests in order to define the particle size and mesh configuration. The brick specimen was numerically simulated under uniaxial compression and tension. The deformed meshes and crack propagation can be observed in Fig. 23 and Fig. 24 for compression and tension, respectively. The cracking between the particles of the material is shown for three increasing loading stages: 80% of the peak load, 100% of peak load, and the ultimate load. The typical progressive failure of the specimen can be observed at different stages under compressive (Fig. 23) and tensile (Fig. 24) loads. In the compressive loading, various micro-cracks appear which are observed to create crack bridging and branching. It can be seen from both figures that the behaviour for the compressive loading is considerably more complex than the behaviour for the tensile loading. It is noted that the shear parameters introduced into the meso-model are of greater importance to the compressive behaviour than the tensile parameters [38].

Similar to the brick calibration, mechanical properties of the mortar were also calibrated. The final values of the meso-model are considered in Table 5, again with the compression values finally inactive.

5.2 Meso-models results

The mesh of continuous elements and interface mesh of the model are presented in Fig. 25. This final meso-model was then subjected to loading and boundary conditions similar to those of the micro-models. After loading, load-displacement data of the model was extracted in a similar location to those extracted from the micro-model and during the experiment with LVDT. The obtained behaviour of the meso-model can then be examined in Fig. 26. Again, the meso-model was considered to be in good agreement with the experimental results.

This meso-model technique becomes of great interest when analysing the failure phenomena because it is able to capture failure at both the interface (as was the case in these experimental tests) and the mortar layer. The meso-model allows to observe and obtain cracks also in the mortar joint. Fig. 27 shows the deformed shapes of the meso-model obtained by lowering the mortar mechanical properties to half. With lower mechanical properties of mortar, in-plane displacement of test unit was larger compared to the same force applied in before mentioned simulations in the elastic regime. Post-peak behaviour was dictated by both the interface properties and properties of mortar. While in the

original model, damage was not observed in the mortar layer, it is clear that with lower properties, the failure occurs in the mortar layer, with the development of several cracks along these joints.

6. Conclusions

Masonry, as an orthotropic composite material, exhibits a multiform, intricated behaviour, which is rather complex to assess numerically and to model due to the various influencing factors. Aspects such as the dimensions of the units and mortar, material properties and arrangement of the brick units can make the assessment and numerical modelling of masonry intricate and variable. The interface between brick units and mortar acts as a plane of weakness and it is the most critical inelastic part for the masonry response. As such, understanding of masonry under shear loading and in situ shear testing is required to create numerically accurate descriptions of masonry and assess masonry structural safety. Different experimental and numerical techniques were adopted here to model and discuss the shear behaviour of masonry.

Furthermore, by considering closely the response obtained in the preliminary test performed at 16th row, it can be deduced that it is essential to gather sufficient data prior to test the in-situ behaviour of the masonry. Challenges and uncertainties involved with materials and testing configurations can negatively impact the results. It is advisable to conduct a thorough investigation before the in-situ experiment to avoid inconclusive or erroneous outcome.

The herein described laboratory experiment has shown that the adoption of digital image correlation to monitor a masonry wall shear test was a very valuable experience because for the first time it was possible to gain an insight into masonry interface behaviour when the brick-mortar composite is undergone to in-plane horizontal loading giving rise to shear damage. The monitored field, focused on the brick test unit and its upper and lower mortar joints, enabled a micro-vision of the real undergoing mechanisms. The plot of novel full-field maps of in-plane displacement and shear strain for the specific test case has allowed the comprehension of the active/not-active sliding interfaces between mortar and brick, as well as the level of material involvement. The maps have shown that the shear strains are well developed along the length of brick-mortar sliding interfaces.

Further, they have shown that the developing shear failure is a very local mechanism, centred along the interfaces and involving very little of the surrounding materials (either brick or mortar). From in-plane

displacement map it became clear that the displacement values vary strongly across active interfaces and not all four interfaces are active. Rather, at least up to maximum shear loading, in this test only the length of one full interface was active per each mortar joint in contact with the test unit. Rotation phenomena of the test unit may likely be a common mechanism in shear failure, in conjunction with the expected lateral sliding of the test unit. Finally, the after-peak information visualised in time-displacement graph pointed to a discontinuous sliding of the test unit, progressing by sudden laceration of portions of the interfaces alternated to rest periods with possible accumulation of additional fracture energy along the interfaces.

The obtained information was both qualitative and quantitative, and it served as input to the numerical modelling. Although the specific test could not provide all necessary mechanical parameter values, it helped the calibration of the computational models. In parallel, the undertaken experiment opened promising perspectives also for improved and less destructive on-site experimental campaigns (for example, with the adoption of method C instead of method A or B reported in the reference testing standard), leading to a better assessment and preservation of URM structures, including historical masonry constructions.

In this paper, a detailed micro-model introduced interfaces as the plane of weakness at the locations of sliding observed during experimental testing. The inelastic phenomena occurring at the interface were modelled using a combined crushing-shearing-cracking (C-S-C) interface constitutive model. The C-S-C introduces a Coulomb-friction model, a tension cut-off and an elliptical compression gap, but also allows a complex model for shear using variable dilatancy. The micro-model adequately represented the experimentally observed response and it is suitable to discuss the shear distribution found in the in-situ shear test. These models are sensitive to the parameters used. For the model presented in this paper, certain critical parameters of interface were identified such as normal and shear stiffness, tensile strength, cohesion and friction angle. However various sets of parameters could be provided to the model, which could yield the same behaviour as the experiment although by vastly different interface data. As such, the parameters chosen for the models must be grounded in reality, based on experimental and theoretical knowledge. In fact, the in-situ shear test must be considered carefully, and different stress levels must be used during experimental campaigns. With a single in-situ shear test, the

information obtained on the joint properties could be insufficient, at least with regard to numerical modelling purposes.

The meso-model utilises particles to represent the materials whilst the particles are joined by inelastic interfaces. Again, the full meso-model was tested and found in agreement with the experimental results. This meso-model technique is of great interest when adopted for these phenomena because it is able to capture failure both at the interface (as it was the case in this experimental test) and in the mortar layer itself.

CRediT author statement:

Pratik N. Gajjar: Numerical Methodology, Formal computational analysis, Writing - Original Draft

Elena Gabrielli: Experimental methodology; Formal experimental analysis, Investigation, Writing - Review & Editing, Supervision

Dafne Carolina Martin-Alarcon: Methodology, Formal computational analysis, Investigation assistance, Writing - Original Draft

João M. Pereira: Numerical Methodology, Formal computational analysis, Writing - Review & Editing, Supervision

Paulo B. Lourenço: Conceptualization, Resources, Writing - Review & Editing, Supervision

Camilla Colla: Conceptualization, Resources, Investigation, Writing - Review & Editing of experimental sections, Supervision

Declaration of competing interest

The authors declare that they have no known competing financial interests or personal relationships that could have appeared to influence the work reported in this paper.

Acknowledgement

The experimental part of this research work has received financial support for materials by the European Commission through the FP7- ENV-2007-1 research project “SMooHS - Smart Monitoring of Historical Structures”, (2008-2011) under grant 212939. The experimental facilities and technical personnel of the LISG laboratory of DICAM Department and of CIRI-EC lab both of the University of Bologna are acknowledged.

The modelling part of this work was partly financed by FCT / MCTES through national funds (PIDDAC) under the R&D Unit Institute for Sustainability and Innovation in Structural Engineering (ISISE), under reference UIDB / 04029/2020.

References

[1] EN 1996-1-1, Design of Masonry Structures-Part 1-1: General Rules for Reinforced and Unreinforced Masonry Structures, European Committee for Standardization, 2005.

[2] G.Vlachakis,E.Vlachaki,P.B.Lourenço, Learning from failure: damage and failure of masonry structures, after the 2017 Lesvos earthquake (Greece), Eng. Fail. Anal. (2020), 104803.

[3] S. Chiostrini, L. Galano, A. Vignoli, On the determination of strength of ancient masonry walls via experimental tests, Proc. of 12th World Conf. Earthquake Eng. (2000).

[4] M. Tomaˇzeviˇc, Shear resistance of masonry walls and Eurocode 6: shear versus tensile strength of masonry, Mater. Struct. 42 (7) (2009) 889–907.

[5] R.H. Atkinson, B.P. Amadei, S. Saeb, S. Sture, Response of masonry bed joints in direct shear, J. Struct. Eng. 115 (9) (1989) 2276–2296.

[6] D. Foppoli, A. Pulcini, A new method to test masonry shear characteristics thought flat jack (FJ-SCT method). Proceedings of the 19th World Conference on Non Destructive Testing, 2016, pp. 13–17. Munich, Germany.

[7] N. Viale, G. Ventura, Shear flat jack test for evaluating shear characteristics on unreinforced masonry structures, Int. J. Architect. Herit. (2020), 1734687.

[8] L. Binda, J. Pina-Henriques, A. Anzani, A. Fontana, P.B. Lourenço, A contribution for the understanding of load-transfer mechanisms in multi-leaf masonry walls: testing and modelling, Eng. Struct. 28 (8) (2006) 1132–1148.

[9] M. Corradi, A. Borri, A. Vignoli, Experimental evaluation of in-plane shear behaviour of masonry walls retrofitted using conventional and innovative methods, Masonry Int. 21 (1) (2008) 29.

[10] B. Silva, M. Dalla Benetta, F. da Porto, C. Modena, Experimental assessment of in- plane behaviour of three-leaf stone masonry walls, Construct. Build. Mater. 53 (2014) 149–161.

[11] P.B. Lourenço, Computational Strategies for Masonry Constructions, Ph. D. thesis, Delft Univ. Press, Delft, The Netherlands, 1996.

[12] P.B. Lourenço, Experimental and Numerical Issues in the Modelling of the Mechanical Behaviour of Masonry. Proc. Structural analysis of historical constructions II, CIMNE, Barcelona, 1998, pp. 57–91.

[13] L. Binda, A. Saisi, Application of NDTs to the Diagnosis of Historic Structures. 7th International Symposium On Nondestructive Testing In Civil Engineering, 2009.

[14] A. Brignola, S. Frumento, S. Lagomarsino, S. Podesta, Identification of shear parameters of masonry panels through the in-situ diagonal compression test, Int. J. Architect. Herit. 3 (1) (2008) 52–73.

[15] A. Zucchini, P.B. Lourenço, A micro-mechanical model for the homogenisation of masonry, Int. J. Solid Struct. 39 (12) (2002) 3233–3255.

[16] A.W. Hendry, Structural Masonry, Macmillan International Higher Education, 1998.

[17] P.B. Lourenço, J.O. Barros, J.T. Oliveira, Shear testing of stack bonded masonry, Construct. Build. Mater. 18 (2) (2004) 125–132.

[18] R. Van der Pluijm, Out-of-plane Bending of Masonry: Behaviour and Strength. Ph.D thesis, Eindhoven University of Technology, The Netherlands, 1999.

[19] ASTM C1531-16, Standard Test Methods for in Situ Measurement of Masonry Mortar Joint Shear Strength Index, ASTM International, West Conshohocken, PA, 2016.

[20] C. Colla, E. Gabrielli, R. Carli, Optical innovative monitoring of masonry testing on site, in: Proc. of AIPND 2015, 16◦ Italian Nat. Conf. on Non-destructive tests, Monitoring and Diagnosis, IDN 10, 2015.

[21] P. Hofmann, S. Stockl, Tests on the shear-bond behaviour in the bed-joints of masonry, Masonry Int. 9 (1986) 1.

[22] EN 1052-3, Methods of Test for Masonry - Part 3: Determination of Initial Shear Strength, European Committee for Standardization, 2004.

[23] E. Gabrielli, C. Colla, Monitoring of weathering effect evolution in porous masonry construction materials: NDT and mechanical tests, Proc. of 9IMC, 9th Int. Masonry Conf. ID1605 (2014) 12.

[24] E. Gabrielli, C. Colla, M. Strojecki, M. Lukomski, Non destructive evaluation of mechanical and environmental decay in masonry structures, in: Proc. AIMETA 2011, XX Conf, Italian Assoc. of Theoretical and Applied Mechanics, 2011, p. 10, in Italian language, “Valutazione non distruttiva

del degrado meccanico e ambientale in strutture murarie".

[25] C. Colla, P.C. Das, D. McCann, M.C. Forde, Sonic, electromagnetic & impulse radar investigation of stone masonry bridges, J. Non-destruct. Test. Eval. Int. 30 (4) (1997) 249–254.

[26] A. Bellini, A. Incerti, M. Bovo, C. Mazzotti, Effectiveness of FRCM reinforcement applied to masonry walls subject to axial force and out-of-plane loads evaluated by experimental and numerical studies, Int. J. Architect. Herit. 12 (3) (2018) 376–394.

[27] E. Gabrielli, C. Colla, Digital image correlation technique for monitoring masonry specimens undergoing mechanical tests, 2013. Proc. AIPnD 2013. IDN 61, (in Italian language, " La tecnica della correlazione digitale di immagini per il monitoraggio di provini di muratura sottoposti a prove meccaniche").

[28] E. Gabrielli, C. Colla, Monitoring of masonry compression tests in the lab via optical correlation without surface preparation, Key Eng. Mater. 624 (2015) 139–146.

[29] E. Gabrielli, C. Colla, Experimental insight in the mechanical behaviour of aged masonry specimens, in: Proc. AIMETA 2015, XXI Conf, Italian Assoc. of Theoretical & Applied Mechanics, 2015, pp. 400–409.

[30] C. Colla, E. Gabrielli, On the response of historic timber beam cross-section when loaded in compression, in: Proc. of SHATIS 2015, 3rd Int. Conf. On Structural Health Assessment of Timber Structures, 2015, pp. 1041–1051.

[31] C. Colla, E. Gabrielli, M. Savoia, Laboratory experience of flood effects monitoring in fired-clay bricks and adobe, Proc. of 9IMC, 9th Int. Masonry Conf. ID1597 (2014) 12.

[32] C. Colla, E. Gabrielli, Photelasticity and DIC as optical techniques for monitoring masonry specimens under mechanical loads, IOP-J. Phys.: Confer. Ser. 778 (1) (2016) 14.

[33] DIANA FEA BV, Diana user's manual, release 10.3, DIANA FEA BV, 2019.

[34] P.B. Lourenço, J.G. Rots, J. Blaauwendraad, Two approaches for the analysis of masonry structures: micro and macro-modeling, Heron 40 (4) (1995) 1995.

[35] P.B. Lourenço, J.G. Rots, Multisurface interface model for analysis of masonry structures, J. Eng. Mech. 123 (7) (1997).

[36] B. Ghiassi, A.T. Vermelfoort, P.B. Lourenço, Masonry mechanical properties, in: B. Ghiassi, G. Milani (Eds.), Numerical Modeling of Masonry and Historical Structures, Woodhead Publishing,

2019, pp. 237–261.

[37] J. Pina-Henriques, Masonry under compression: failure analysis and long-term effects. Ph.D dissertation, Universidade do Minho, Portugal, 2005.

[38] P.B. Lourenço, J. Pina-Henriques, Validation of analytical and continuum numerical methods for estimating the compressive strength of masonry, Comput. Struct. 84 (29–30) (2006) 1977–1989.

Tables

Table 1 - Measurement of the brick unit and mortar dimensions (all in mm)

Dimension	Nominal	On test unit
Brick length	250	246
Brick width	120	118
Brick height	55	54
Mortar joint thickness	10	9

Table 2 - Mechanical properties of brick and mortar [23]

Property	Brick	Mortar
Compressive strength (MPa)	80	3.2
Elastic modulus (GPa)	16	4.8
Bending strength (MPa)	-	1.2

Table 3 - Mechanical properties of the brick masonry [24]

Property	Brick Masonry
Compressive strength (MPa)	16
Elastic modulus (GPa)	3.1
Poisson's ratio (-)	0.13
Shear modulus (GPa)	1.6

Table 4 - C-S-C interface model properties

Description	Values
Normal stiffness (N/mm^3)	100
Shear stiffness (N/mm^3)	45
Tensile strength (N/mm^2)	2.1
Tensile fracture energy (N/mm)	0.1
Cohesion (N/mm^2)	2.1
Tangent of friction angle	0.75
Tangent of dilatancy angle	0.02
Tangent of residual friction angle	1.0
Confining normal stress (N/mm^2)	-7.0
Exponential degradation parameter	1.0
Shear fracture energy (N/mm)	6.0

Table 5 - Material Properties used for Meso-model

Property	Brick	Mortar	Brick-Mortar interface
Elastic modulus (kN/mm^2)	16000	4800	-
Poisson's ratio (-)	0.13	0.13	-
Tensile strength (N/mm^2)	8.0	0.5	2.1
Tensile fracture energy (N/mm)	0.5	0.05	0.1
Cohesion (N/mm^2)	6.0	0.6	1.9
Shear fracture energy (N/mm)	6.0	0.6	6.0
Tangent of friction angle	0.7	0.7	0.75
Tangent of dilatancy angle	0.01	0.01	0.01

Figures

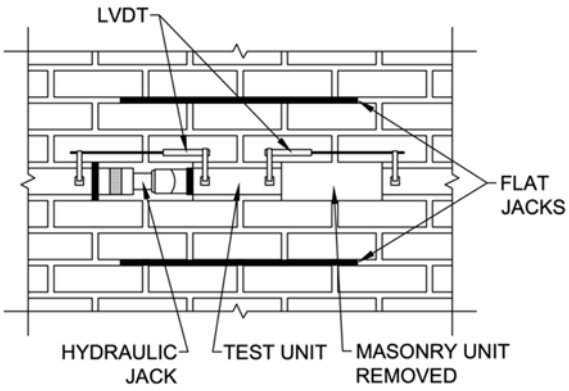

Fig. 1 - Schematic of masonry shear testing according to ASTM C1531 Method A (modified from ASTM C1531-16, 2016)

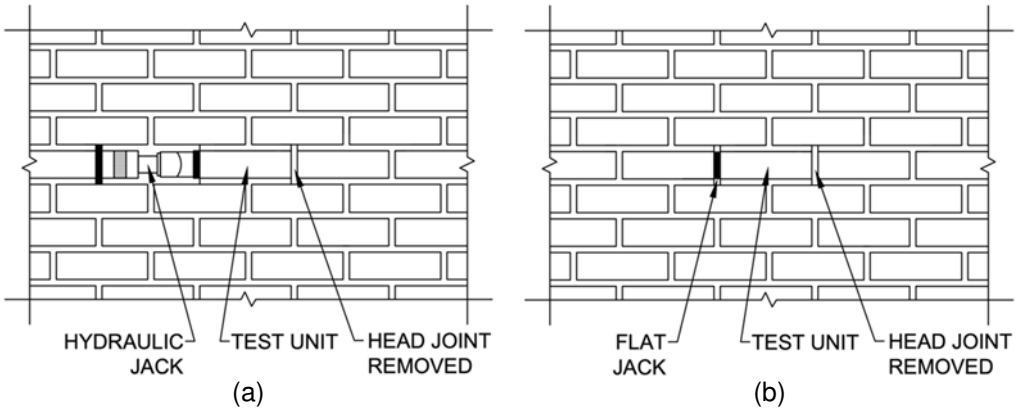

Fig. 2 - Schematic of masonry shear testing according to ASTM C1531: a) Method B; b) Method C (modified from ASTM C1531-16, 2016).

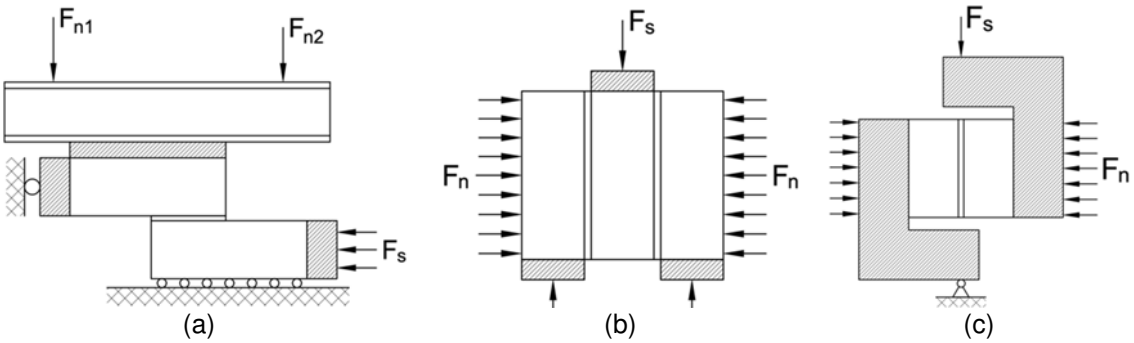

Fig. 3 - Shear test experimental setups: a) Couplet test; b) Triplet test; c) Van der Plujim test [17]

(a) (b)

Fig. 4 - Demolition of mortar joints by drilling around the bricks would precede the removal of the brick to the sides of the test unit before placing the jack and applying the shear force.

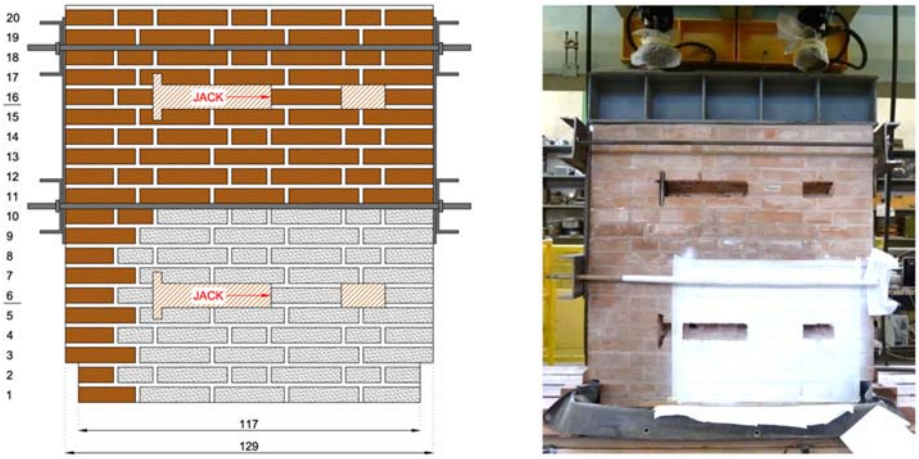

(a) (b)

Fig. 5 - Experimental setup of the masonry wall: a) schematics of the originally planned and prepared test locations. Setup at course six was later modified; b) masonry specimen with top and bottom stiff beams for distribution of vertical load.

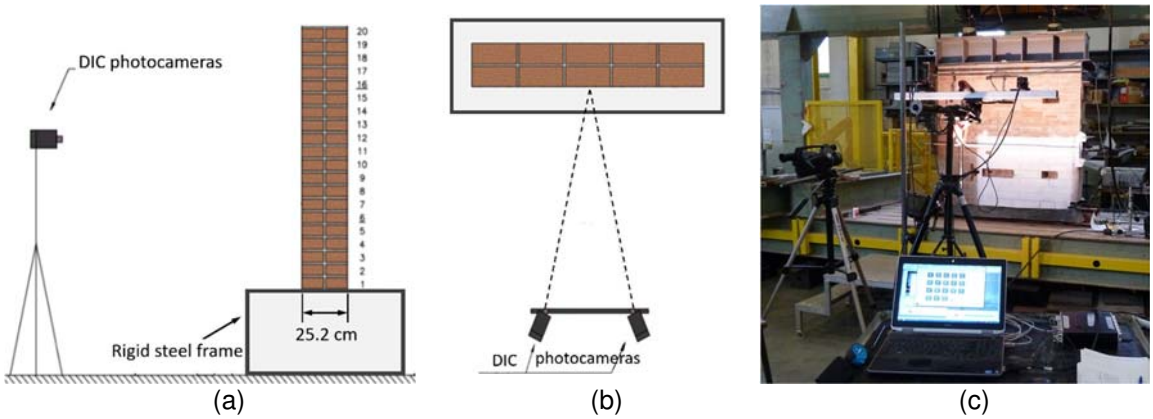

(a) (b) (c)

Fig. 6 - Test setup with DIC system: a) lateral view; b) plan view; c) full test setup

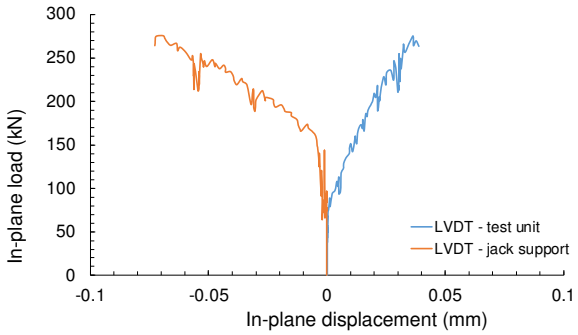

Fig. 7 - Horizontal load-displacement graph for the tested brick unit of the shear test at course 16 of the wall. Small displacements are measured (approx. 0.075 mm and 0.04 mm for each of the 2 LVDTs) for a considerable peak load (279 kN) before sudden failure.

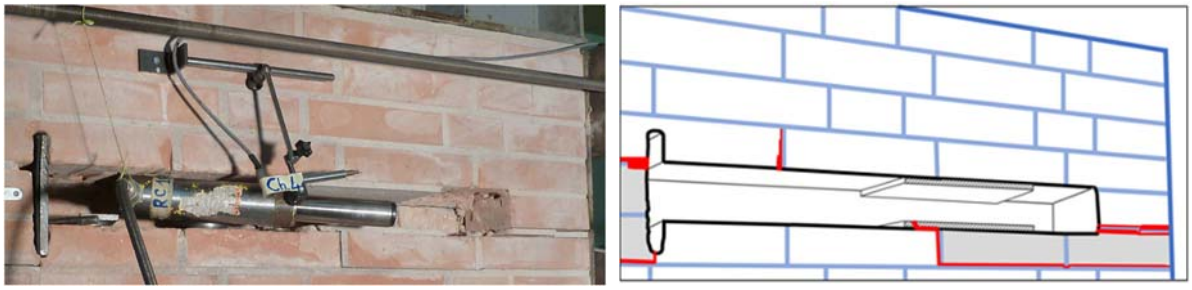

(a) (b)

Fig. 8 - Explosive shear failure with brick expulsion at brick course 16: (a) view of obtained damage with the displaced and fully extended hydraulic jack also occupying the space of the test unit, the 2 “clean” bed joints where the test unit was; the front LVDT and its support hanging loose, three bricklayers above course 16, and to the extreme left, the steel plate at the rear of the jack is still in place: (b) survey of the crack pattern is shown in red; bricks which have suffered out-of-plane displacement are shown in grey colour

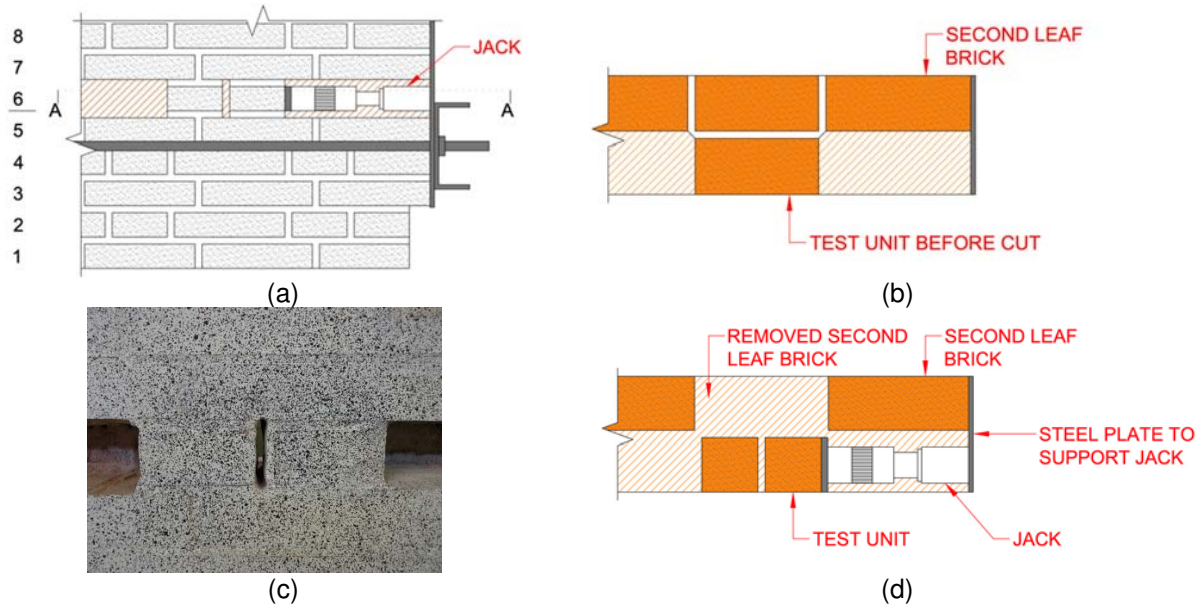

(a) (b)

(c) (d)

Fig. 9 - Schematics of test setup at the wall’s 6th layer: a) detail of front view with A-A section position; b) temporary A-A horizontal longitudinal wall section at 6th layer after removal of only two bricks at test unit’s sides; c) close-up detail of front view after removal of brick at rear leaf and after halving the test unit by a vertical groove. The surface was then prepared for optical monitoring; d) A-A horizontal wall section, showing a final brick configuration and jack insertion

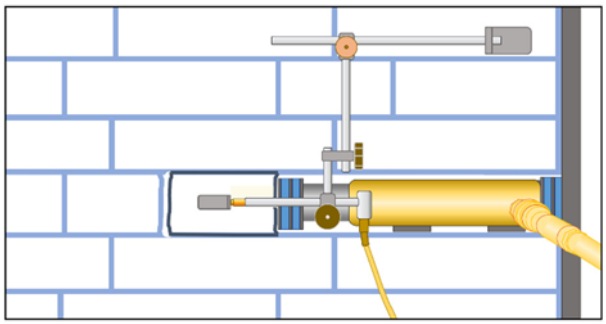

Fig. 10 - Scheme of test setup at the wall's 6th layer with LVDT tip resting at the middle of the test brick front surface and hydraulic jack resting with back against the steel plate

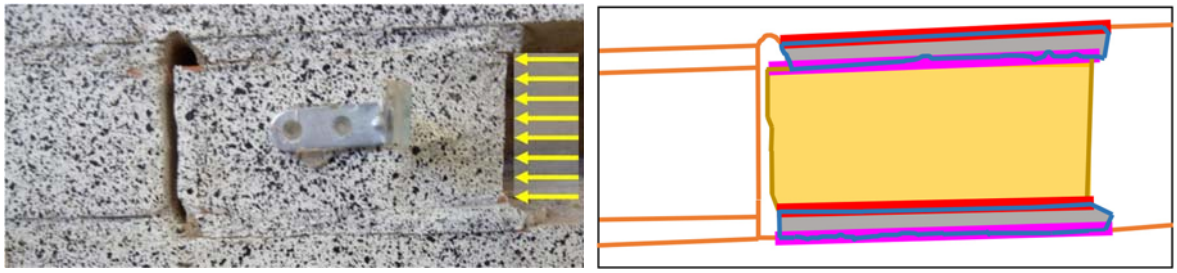

(a) (b)

Fig. 11 - Shear failure of the test unit and the brick-mortar interfaces: (a) photo shot at the end of brick sliding. In the centre of the test unit it is visible a base point for LVDT readings. Yellow arrows show direction and area of applied shear load; (b) scheme highlighting the final deformed configuration of test unit (in amber colour) and mortar joints (in grey). The two active interfaces are highlighted in pink. The distortion visible in the image (lines not horizontal) is only replicating the perspective view of the photo in (a).

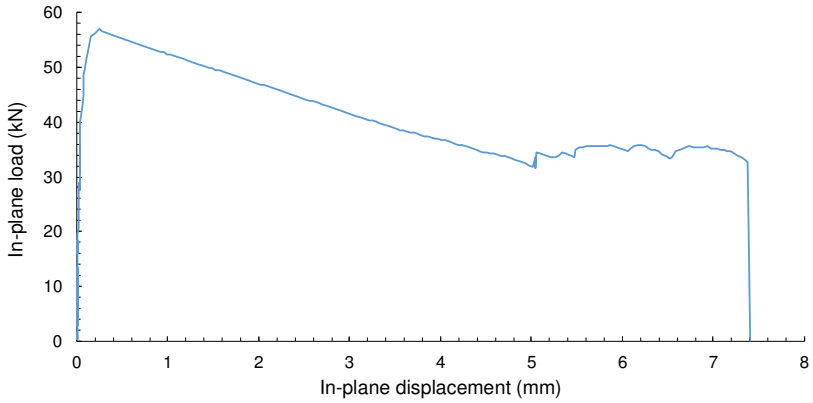

Fig. 12 - Load-displacement graph of the tested brick unit at course 6 of the wall. The shown displacement values are recorded via the applied front LVDT. A displacement of 0.27 mm is recorded at a peak load of 57 kN, whilst total sliding is 7.4 mm.

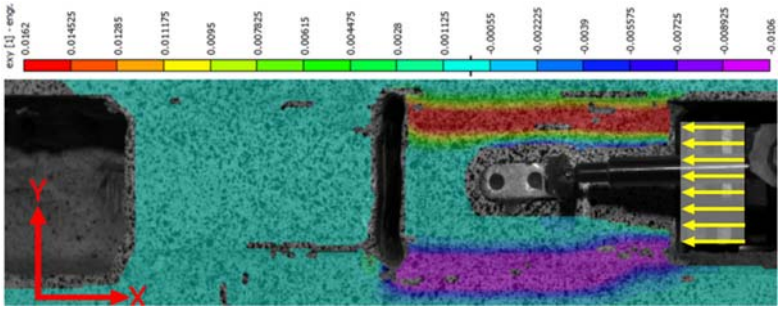

Fig. 13 - DIC mapping of shear strain at maximum loading of the test unit at course 6th (in the right half of the image)

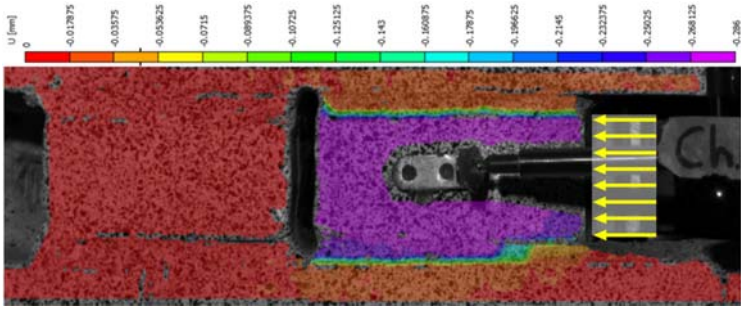

Fig. 14 - DIC mapping of in-plane displacement at a time instant close to maximum loading for the test at course 6th (legend values shown in millimetres). Red colour shows no or minimal displacement; the purple colour maximum value is equal to 0.286 mm

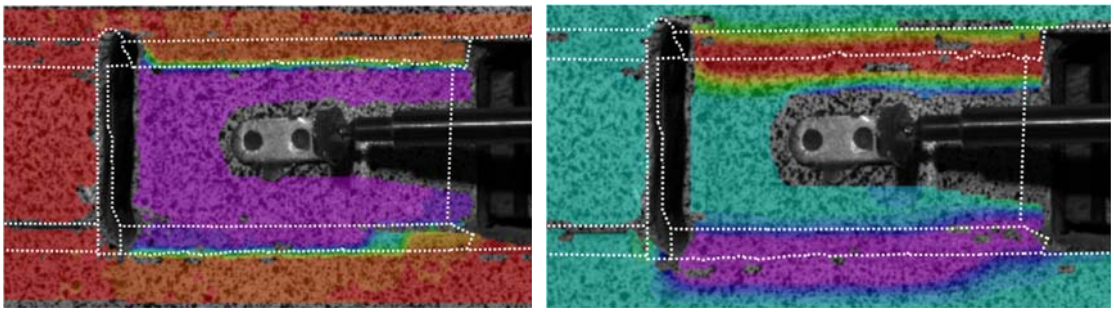

(a) (b)

Fig. 15 - Direct comparison of DIC in-plane displacement (a) and shear strain maps (b) at maximum loading. The geometry at the end-of-recording is overlaid to maps as dotted white lines to identify interface positions better.

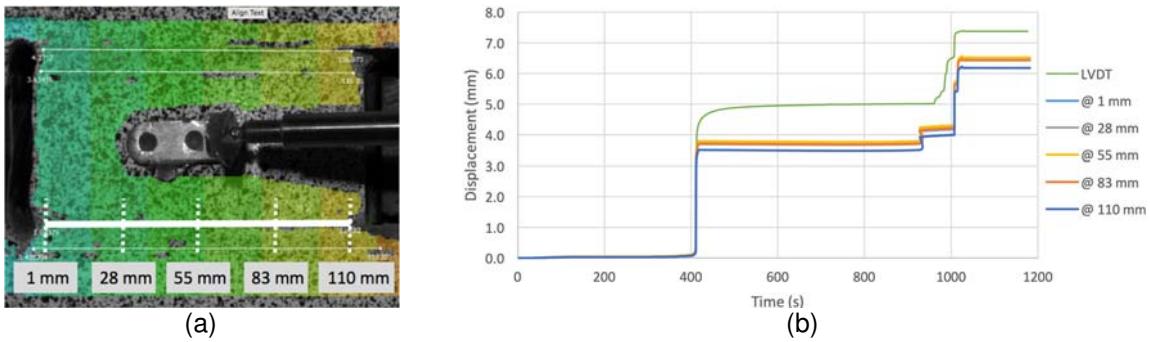

(a) (b)

Fig. 16 - DIC and LVDT in-plane displacement values comparison for the test at course 6th: a) extraction of DIC points along interface marked by a thick white line, whilst LVDT base point is fixed at mid-height of test unit; b) time-displacement plot of in-plane displacements

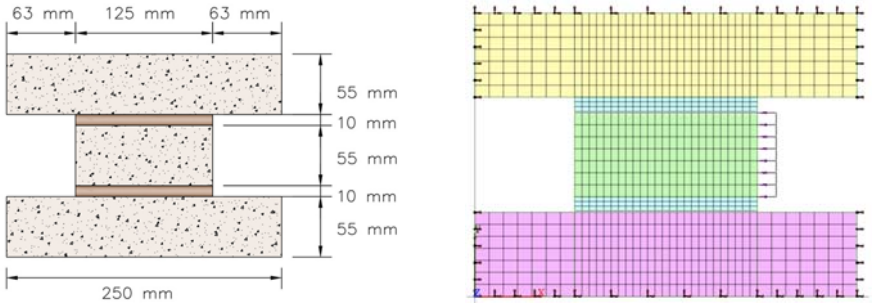

Fig. 17 - Numerical model: a) model geometry; b) boundary conditions

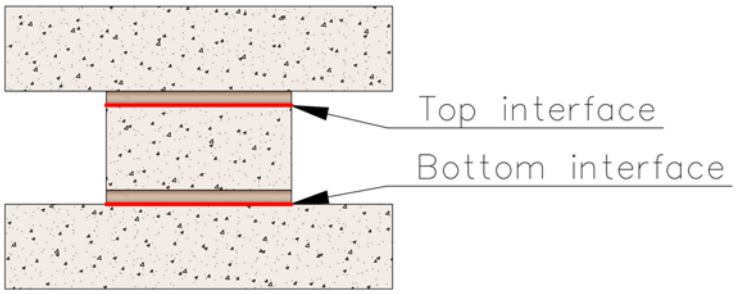

Fig. 18 - Model's interface elements

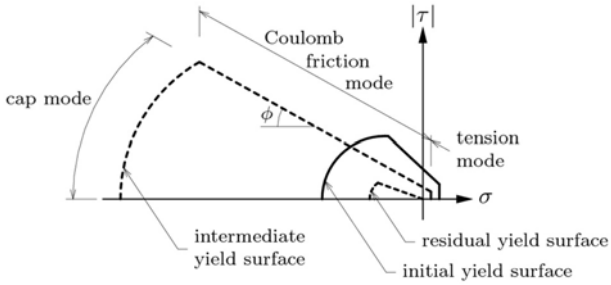

Fig. 19 - 2D combined C-S-C interface model [26]

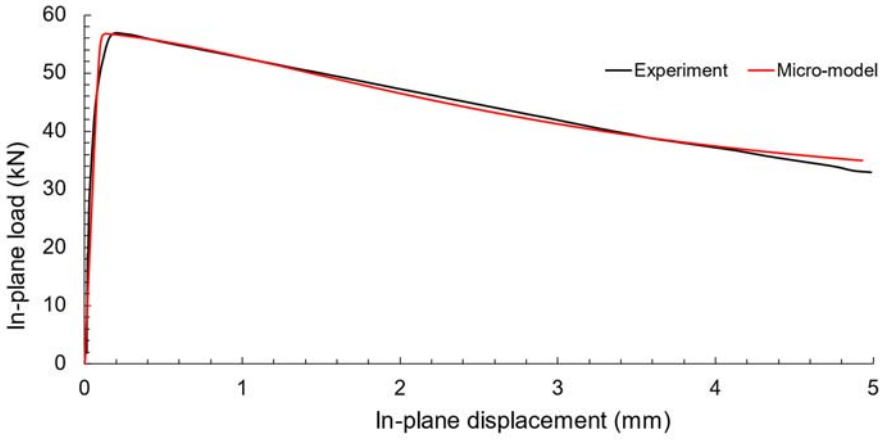

Figure 20 - Load-Displacement diagram of micro-model and experiment

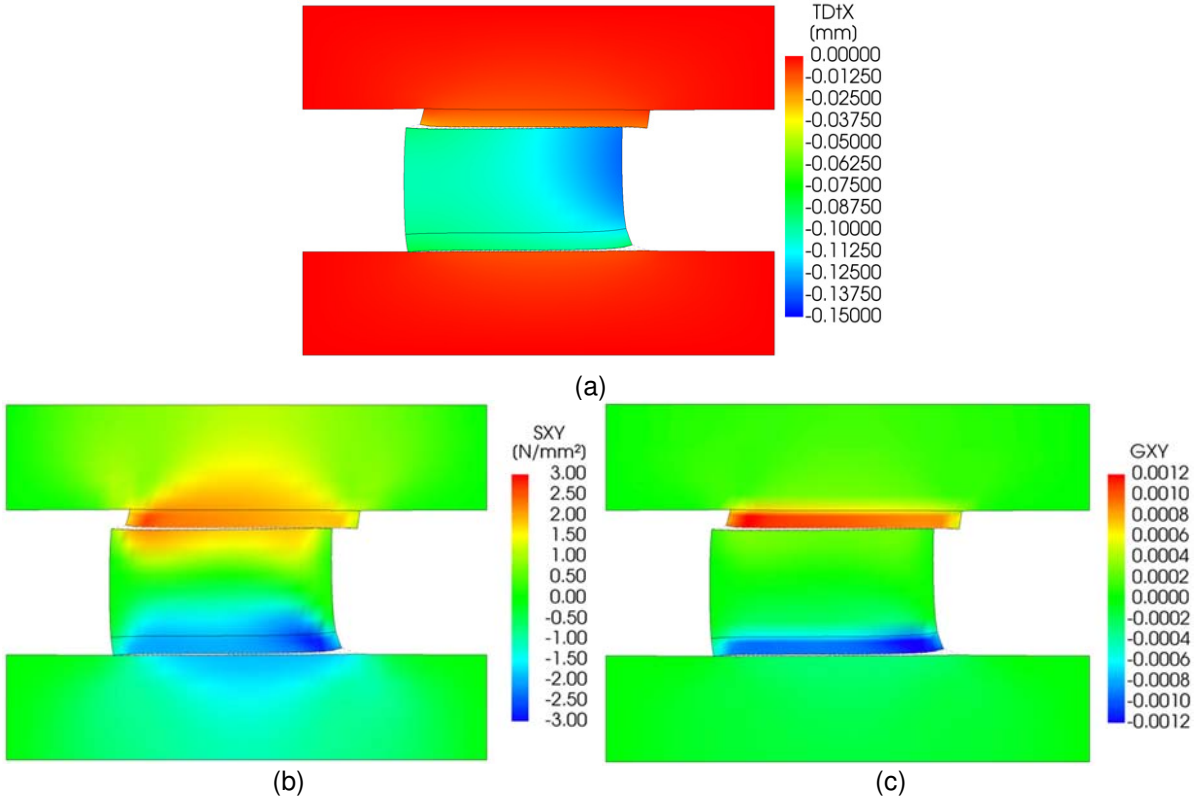

Fig. 21 - Analysis results of micro-model at peak shear force: a) in-plane displacement; b) shear stress; c) shear strain

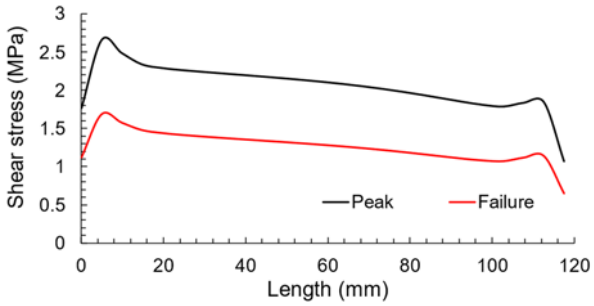

Figure 22 - Shear stress distribution along with the upper interface

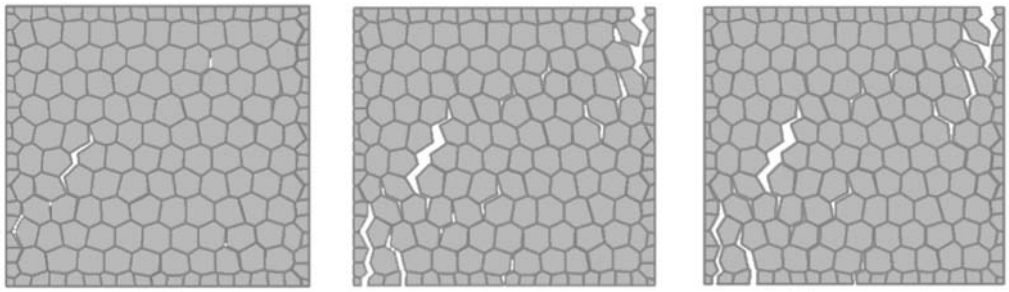

Fig. 23 - Brick uniaxial compression: a) 80% peak stress; b) peak stress; c) final stage

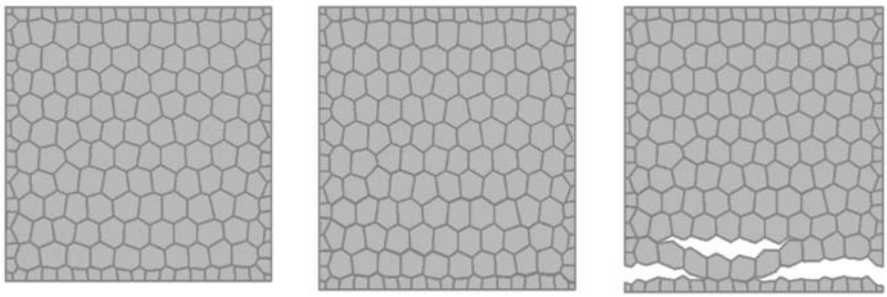

(a) (b) (c)

Fig. 24 - Brick uniaxial tension: a) 80% peak stress; b) peak stress; c) final stage

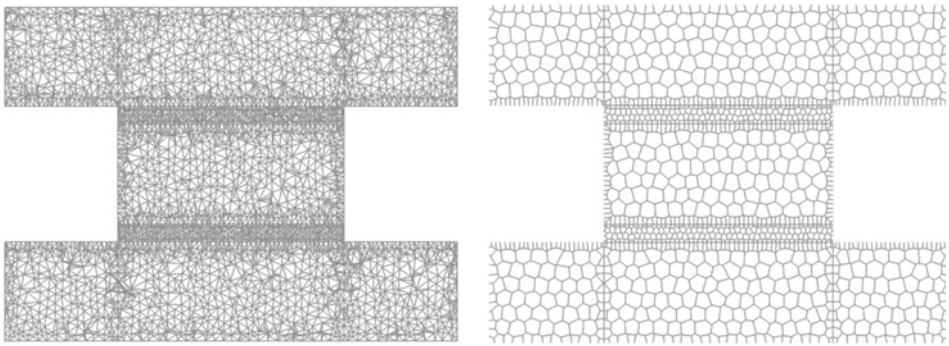

(a) (b)

Fig. 25 - Meso-model: a) continuous elements mesh; b) interface elements mesh.

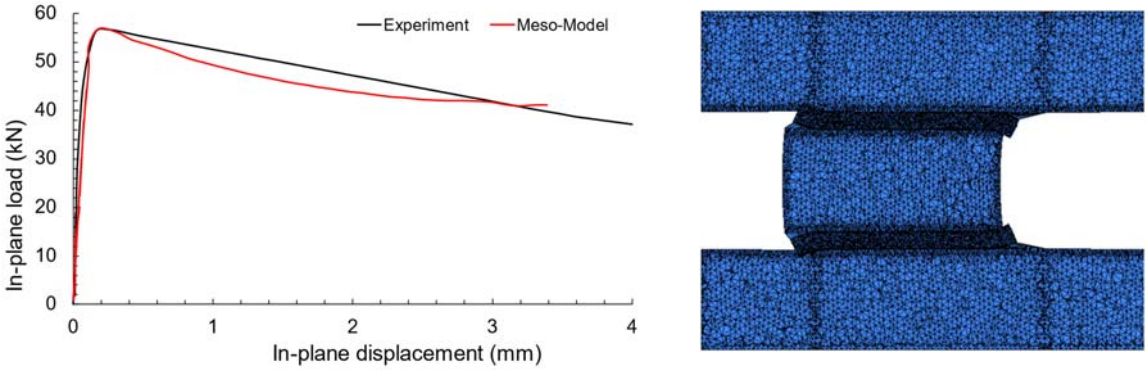

(a) (b)

Fig. 26 - Meso-model results: a) load-displacement profile; b) in-plane displacement at failure

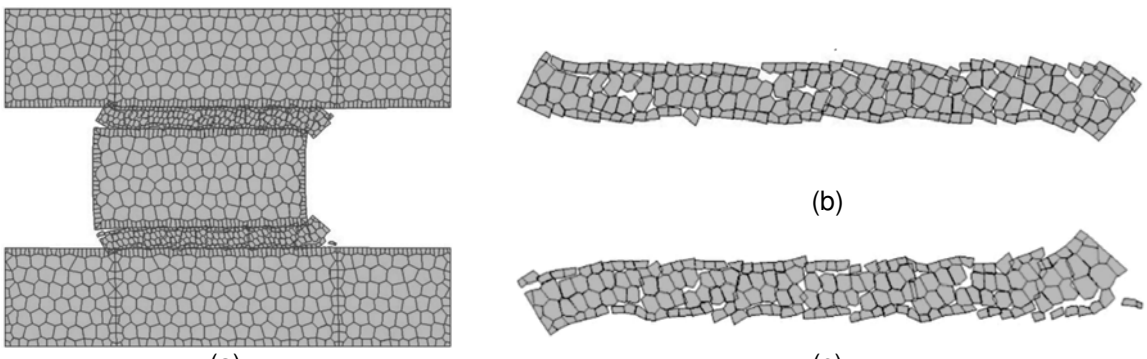

(a) (b) (c)

Fig. 27 - Example of meso-model with failure in the mortar joint: a) full deformed shape; b) top mortar joint; c) bottom mortar joint.